Macedonian Journal of Chemistry and Chemical Engineering, Vol. **45**, No. 2, pp. xx–xx (2026)

MJCCA9 –

ISSN 1857-5552
e-ISSN 1857-5625

Received: June 12, 2026
Accepted: August 28, 2026

DOI: 10.20450/mjcce.2026.3579
Original scientific paper

UREA–CARBON NANOTUBE COMPOSITES: SYNTHESIS, CHARACTERIZATION, AND DIFFERENTIAL ANTIBACTERIAL ACTIVITY AGAINST *STAPHYLOCOCCUS AUREUS* AND *ESCHERICHIA COLI*

Qadoori Zedan Khalaf[1], Kareem Jumaah Jibrael Al-Salihi[2*], Mahir Essa Al-Salihi[3]

[1]Department of Chemistry, College of Education, Al-Iraqia University, Iraq
[2]Department of Chemistry, College of Science, University of Sulaimani, Sulaymaniyah, Iraq
[3]Medical Laboratory Technology Department, Kifri Technical Institute, Garmian Polytechnic University, Kifri, Iraq

kareem.jibrael@univsul.edu.iq

This study focuses on the synthesis, characterization, and antibacterial assessment of urea-functionalized carbon nanotube (CNT) composites. Amide nanotubes can be formed through the self-assembly of amphiphilic molecules driven by hydrogen-bonding interactions; however, previously reported approaches may be limited by aggregation and difficulties in large-scale production. In the present work, CNTs were functionalized with urea and systematically characterized using Fourier-transform infrared spectroscopy, X-ray diffraction, X-ray photoelectron spectroscopy (XPS), thermogravimetric analysis, scanning electron microscopy, atomic force microscopy, and measurement of the zeta potential to evaluate their structural, chemical, thermal, morphological, and surface-charge properties. The results demonstrated the incorporation of urea-derived functionalities onto the CNT surface. Although functionalization decreased the thermal stability of the CNTs, the spectroscopic results indicated the presence of amide-related functional groups in the CNT–urea–CNT composite. Among the characterization techniques, XPS provided direct evidence of urea incorporation through the appearance of the N 1s signal and corresponding changes in the C 1s and O 1s spectra. Collectively, these results demonstrate substantial modification of the CNT surface following treatment with urea, without implying definitive covalent attachment. Measurement of the zeta potential further revealed a substantial alteration in the surface-charge behavior following functionalization. As pH increased, the zeta potential progressively decreased, a phenomenon that can be attributed to the deprotonation of surface functional groups. Pristine CNTs exhibited an isoelectric point (IEP) at approximately pH 7–8, whereas urea functionalization shifted the IEP to around pH 4, indicating a significant modification of the CNT surface chemistry. The urea–CNT and CNT–urea–CNT composites exhibited concentration-dependent antibacterial activity against *Staphylococcus aureus* and *Escherichia coli* at 0.01–0.1 mg mL^{-1}. The CNT–urea–CNT composite was more active against *S. aureus* at 0.05 and 0.1 mg mL^{-1}, while the urea–CNT composite showed greater activity at 0.01 mg mL^{-1}. The CNT–urea–CNT composite consistently exhibited stronger activity against *E. coli*, with a maximum inhibition zone of 33 ± 3.01 mm at 0.1 mg mL^{-1}. These differences may reflect variations in surface structure, dispersion, and interactions with bacterial membranes.

Keywords: urea; carbon nanotubes; composite materials; antibacterial activity

КОМПОЗИТИ НА УРЕА И ЈАГЛЕРОДНИ НАНОЦЕВКИ: СИНТЕЗА, КАРАКТЕРИЗАЦИЈА И РАЗЛИЧНА АНТИБАКТЕРИСКА АКТИВНОСТ ПРОТИВ *STAPHYLOCOCCUS AUREUS* И *ESCHERICHIA COLI*

Ова истражување се фокусира на синтезата, карактеризацијата и испитувањето на антибактериската активност на композити од јаглеродни наноцевки (CNT) функционализирани со уреа. Амидните наноцевки можат да се формираат преку самоорганизација на амфифилни

молекули, поттикната од интеракции со водородни врски. Сепак, претходно објавените пристапи можат да бидат ограничени поради агрегацијата и тешкотиите поврзани со производството во поголем обем. Во ова истражување, јаглеродните наноцевки беа функционализирани со уреа и систематски карактеризирани со примена на инфрацрвена спектроскопија со Фуриеова трансформација (FTIR), рендгенска дифракција (XRD), рендгенска фотоелектронска спектроскопија (XPS), термогравиметриска анализа (TGA), скенирачка електронска микроскопија (SEM), микроскопија на атомски сили (AFM) и мерење на зета-потенцијалот, со цел да се испитаат нивните структурни, хемиски, термички, морфолошки својства и својствата на површинскиот полнеж. Резултатите покажаа инкорпорирање на функционални групи изведени од уреа на површината на јаглеродните наноцевки. Иако функционализацијата ја намали термичката стабилност на наноцевките, спектроскопските резултати укажаа на присуство на функционални групи поврзани со амидната група во композитот CNT–urea–CNT. Од применетите техники за карактеризација, XPS обезбеди директен доказ за инкорпорирањето на уреата преку појавата на сигналот N 1s и соодветните промени во спектрите C 1s и O 1s. Севкупно, овие резултати укажуваат на значителна модификација на површината на јаглеродните наноцевки по третманот со уреа, без притоа да се имплицира дефинитивно ковалентно поврзување. Мерењето на зета-потенцијалот дополнително откри значителна промена во однесувањето на површинскиот полнеж по функционализацијата. Со зголемување на pH-вредноста, зета-потенцијалот постепено се намалуваше, што може да се припише на депротонирањето на површинските функционални групи. Кај нефункционализираните јаглеродни наноцевки беше забележана изоелектрична точка (IEP) при pH 7–8, додека функционализацијата со уреа ја помести IEP до приближно pH 4, што укажува на значителна промена во површинската хемија на наноцевките. Композитите уреа–CNT и CNT–уреа–CNT покажаа концентрационо зависна антибактериска активност против *Staphylococcus aureus* и *Escherichia coli* при концентрации од 0,01 до 0,1 mg^{-1}. Композитот CNT–уреа–CNT покажа поголема активност против *S. aureus* при концентрации од 0,05 и 0,1 mg mL^{-1}, додека композитот уреа–CNT покажа поголема активност при концентрација од 0,01 mg mL^{-1}. Композитот CNT–уреа–CNT доследно покажа посилна активност против *E. coli*, со максимална зона на инхибиција од 33 ± 3,01 mm при концентрација од 0,1 mg mL^{-1}. Овие разлики може да се должат на варијациите во површинската структура, дисперзноста и интеракциите со бактериските мембрани.

Клучни зборови: уреа; јаглеродни наноцевки; композитни материјали; антибактериска активност

1. INTRODUCTION

Carbon nanotubes (CNTs) are considered one of the most promising nanomaterials due to their exceptional mechanical strength, high surface area, electrical conductivity, and chemical stability, making them suitable for a wide range of applications, including in nanomedicine and antimicrobial therapies.[1,2] However, pristine CNTs often exhibit limited solubility and biocompatibility, and their biological properties must be evaluated by considering potential toxicity.[3] Functionalization of CNTs, particularly through covalent and noncovalent modifications, is a widely employed strategy to overcome these limitations and improve their dispersion, stability, and targeted activity.[3] Among various functionalization approaches, amide-based modifications have attracted significant attention due to the strong hydrogen bonding capabilities and structural compatibility with biological molecules.[4] Amide linkages can be introduced onto the surface of CNTs through reactions with carboxyl or amine groups, allowing for the design of nanotube-based composites with improved bio-interactions and antibacterial activity.[5]

The growing threat of bacterial resistance has intensified the search for novel antimicrobial materials with enhanced efficacy and biocompatibility.[6] Among the various nanomaterials explored, CNTs have garnered significant attention due to their unique structural, electrical, and mechanical properties, as well as their potential for functional modification.[7,8] Surface engineering of CNTs with bioactive molecules can significantly improve their interaction with microbial cells, thereby enhancing their antibacterial capabilities.[8] Amide-based functionalization, particularly with urea and diamide groups, offers a promising strategy for modifying CNTs through hydrogen bonding and self-assembly mechanisms, leading to well-defined nanotubular structures.[9] However, challenges such as aggregation and limited scalability remain barriers to their widespread application. These functionalized CNTs can interact with bacterial cell membranes, potentially leading to membrane disruption, oxidative stress, and cell death, especially in pathogenic bacteria such as

Staphylococcus aureus and *Escherichia coli*.[10] Modifying the physicochemical properties of CNTs has been shown to significantly influence their cytotoxic effects in bacterial systems.[11] These findings highlight the importance of accurately documenting both physical and chemical characteristics when assessing the toxicity of carbon-based nanomaterials.[12] Studies have revealed that all CNT variants exhibit notable antimicrobial activity, although they differ in their capacity to induce oxidative stress and reduce colony-forming units (CFU) across various microbial species.[13] Several parameters affect the antibacterial efficacy of CNTs, including their size (diameter and length), degree of aggregation, surface functionality, concentration, buffer environment, exposure time and intensity, and the specific bacterial strain involved.[14]

CNTs and related carbon nanomaterials have attracted considerable attention because of their strong antibacterial properties. Functionalized multi-walled CNTs demonstrated effective antimicrobial activity against both *E. coli* and *S. aureus*, with optimal inhibition observed at concentrations of 80 and 60 μg mL^{-1}, respectively.[15] Their antibacterial behavior is mainly associated with membrane disruption and oxidative stress mechanisms, which are also reported for graphene-based nanomaterials.[16]

CNT-based and graphene-derived nanocomposites further enhance antibacterial efficiency through synergistic interactions with metals and polymers. For example, reduced graphene oxide–silver nanoparticle composites showed strong activity against *Proteus mirabilis*, *S. aureus*, and *E. coli,* outperforming nitrofurantoin in some cases because of rapid membrane damage and oxidative stress effects.[17] The highest antimicrobial activity was shown by nanodiamonds, carbo nanofibers and carboxylated hydrophilic multi-walled CNTs.[18] In addition, carbon nanoparticles synthesized from glucose displayed hydrophilic and fluorescent properties due to hydroxyl-rich surfaces, demonstrating the versatility of carbon nanostructures for functional and biomedical applications.[19] Overall, these studies emphasize the growing importance of CNTs and carbon-based nanocomposites as promising alternatives to conventional antibacterial materials.

This study presents the synthesis of two urea-functionalized CNT composites, their characterization, and evaluation of their antibacterial activity against a gram-positive bacterium (*S. aureus*) and a gram-negative bacterium (*E. coli*). The novelty of this study lies in correlating the structural modification of CNTs with their antibacterial properties while assessing their potential suitability for biomedical antimicrobial applications.

2. EXPERIMENTAL

2.1. *Chemicals and materials*

Multi-walled CNTs (thin, > 8 % carboxylic acid functionalized, O.D. × L 7–15 nm × 0.5–10 μm) were purchased from Sigma-Aldrich, St. Louis, Missouri, USA). Urea (purity 99.5 %) was obtained from VWR Chemicals. LLC (Solon, OH, USA).

Lyophilized certified reference strains *S. aureus* ATCC 25923 (gram positive) and *E. coli* ATCC 25922 (gram-negative) were obtained from American Type Culture Collection (ATCC, Manassas, VA, USA). The strains were reconstituted and maintained according to the supplier's instructions before use. To assess antibacterial activity, fresh bacterial suspensions were prepared in sterile physiological saline and adjusted to 0.5 McFarland standard (approximately 1.5×10^8 CFU mL^{-1}). Mueller–Hinton agar was used for the disk-diffusion assays.

2.2. *Synthesis of the urea–CNT composite*

This procedure was adapted from the method described by Saeed et al.[20] One gram of urea was dissolved in 20 mL of ethanol with stirring to ensure complete dissolution. Then, 1 g of wrapped CNTs were added to the urea–ethanol solution. The mixture was heated with continuous stirring under reflux for 2 hours to promote homogeneity and reaction between urea and CNTs. The produced precipitate was filtered and then washed with ethanol to eliminate any unreacted substances or impurities. Finally, the purified product was dried at 60 °C to remove residual ethanol and obtain the final amide derivative.

2.3. *Synthesis of the CNT–urea–CNT composite*

Approximately 0.5 g of urea–CNT composite was added to a round-bottom flask, followed by 20 mL of ethanol and 1.0 g of CNTs. The mixture was heated under reflux for 2 hours with continuous stirring. After completion of the reaction, the resulting product was collected and dried at 60 °C.

2.4. *Characterization*

2.4.1. *X-ray diffraction (XRD)*

XRD analysis was performed to identify the crystalline phases, determine the crystal structure, and evaluate the crystallinity of the synthesized material. The XRD pattern was recorded using a D/MAX-rA X-ray diffractometer (Rigaku Corporation, Tokyo, Japan) with Cu Kα radiation (λ = 0.15418 nm). The sample was scanned over a 2θ range of 3° to 80° at a scan rate of 1° minute^{-1}.

2.4.2. *Fourier-transform infrared (FTIR) spectroscopy*

FTIR spectroscopy was used to identify the functional groups present in the sample and to confirm the chemical bonding and surface interactions of the synthesized material. The samples were finely ground, mixed with KBr, and pressed into pellets. FTIR spectra were recorded in the range of 500–4000 cm^{-1} at a resolution of 2 cm^{-1} using a Tensor 27 FTIR spectrometer (Bruker Corporation, Ettlingen, Germany).

2.4.3. *X-ray photoelectron spectroscopy (XPS)*

XPS was used to examine the surface chemical and elemental composition of the prepared materials. The measurements were performed using an ESCALAB Xi+ X-ray photoelectron spectrometer (Thermo Fisher Scientific, East Grinstead, West Sussex, UK) equipped with a monochromatic Al Kα X-ray source ($h\nu$ = 1486.6 eV). The analysis was conducted under high-vacuum conditions, and the survey spectra were recorded over an appropriate binding-energy range to identify the elements present on the sample surface. High-resolution spectra of the relevant core-level regions, including C 1s, O 1s, N 1s, and other characteristic elements, were subsequently acquired to determine their chemical environments.

2.4.4. *Thermogravimetric analysis (TGA)*

TGA was performed to evaluate the thermal stability, decomposition behavior, and residual mass of the prepared composites. Approximately 5–10 mg of each sample was placed in a ceramic/alumina crucible and analyzed using a TGA/DSC thermogravimetric analyzer (Mettler Toledo, Greifensee, Switzerland). The measurements were conducted under a controlled nitrogen atmosphere at a flow rate of approximately 50 mL minute^{-1}. The samples were heated from 25 to 800 °C at a constant heating rate of 10 °C minute^{-1}.

2.4.5. *Scanning electron microscopy (SEM)*

A scanning electron microscope (JSM-IT510, JEOL Ltd., Akishima, Tokyo, Japan) was used to examine the particle shape, surface texture, and the degree of agglomeration at high magnification of the composites. Prior to imaging, the samples were carefully dried and mounted onto aluminum stubs using conductive carbon tape to ensure proper adhesion and electrical grounding. To minimize charging effects during observation, a thin conductive layer of gold or platinum was deposited on the sample surface using a sputter coater. SEM was carried out under high-vacuum conditions at an accelerating voltage typically ranging from 5 to 20 kV, depending on the sample's conductivity and desired resolution. Both secondary electron and backscattered electron detectors were used to obtain detailed topographical and compositional contrast images.

2.4.6. *Atomic force microscopy (AFM)*

AFM was employed to investigate the surface morphology and nanoscale structural features of the composites. A MultiMode 8 AFM system (Bruker Corporation) operating in tapping mode under ambient conditions was used. The samples were prepared by drop-casting dilute dispersions onto freshly cleaved mica substrates and allowing them to dry prior to analysis.

2.5. *Determination of the zeta potential*

The zeta potential of pristine CNTs and the prepared composites was measured using a Zetasizer Nano ZS (Malvern Instruments Ltd., Malvern, UK). For sample preparation, CNTs were dispersed in deionized water at a concentration of 0.1 mg mL^{-1}. A constant ionic strength was maintained throughout the measurements by using a 1 mM sodium chloride (NaCl) electrolyte solution. The resulting suspension was subjected to ultrasonication for 30 minutes to achieve uniform particle dispersion and reduce aggregation. The pH of the CNT dispersion was adjusted over the range of 3–11 using 0.1 M hydrochloric acid (HCl) and 0.1 M sodium hydroxide (NaOH). Following pH adjustment, the suspension was transferred into disposable folded capillary cells designed for zeta potential analysis.

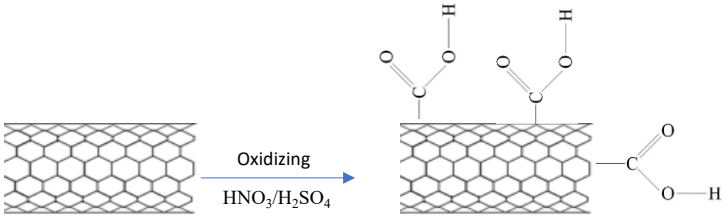
2.6. *Antibacterial activity*

The antibacterial activity of the composites was evaluated using the disk diffusion method,[21] performed using the agar well diffusion (pitting) method on prepared Mueller–Hinton agar. Microbial suspensions of *S. aureus* and *E. coli* were prepared and adjusted to match a 0.5 McFarland standard, corresponding to a bacterial concentration of 1.5×10^8 CFU mL^{-1}. The agar plates were uniformly inoculated with the microbial suspensions using sterile cotton swabs. Swabbing was performed three times over the agar surface, with the plate rotated by 60° after each swabbing to ensure even distribution. The plates were then allowed to dry at room temperature. Five wells were aseptically punched into the agar using a sterile cork borer. Each well was filled with 80 µL of the appropriate composite at different concentrations (0.01, 0.05, and 0.1 mg mL^{-1}); deionized water served as the negative control[22]. The plates were incubated at 37 °C for 24 hours. After incubation, the inhibition zones were measured in mm^2. All experiments were performed in triplicate

3. RESULTS AND DISCUSSION

The present study demonstrates that functionalization of CNTs with urea provides an effective approach for modifying their surface chemistry and enhancing their antibacterial properties. The incorporation of urea onto the CNT surface was supported by the complementary structural and physicochemical characterization results. Compared with pristine CNTs, urea-functionalized CNTs exhibited changes in their surface composition, thermal behavior, crystallinity, and interfacial properties, indicating successful interaction between the urea molecules and the nanotube surface.[23] These modifications are particularly important because the biological activity of CNT-based materials is strongly dependent on their surface chemistry, dispersion, surface charge, and interaction with microbial cells.

Pristine CNTs consist predominantly of sp^2-hybridized carbon atoms arranged in a graphitic structure, which gives them excellent electrical, thermal, and mechanical properties but also results in poor dispersibility in many polar solvents and weak interfacial interaction with polymeric or inorganic matrices.[24] Treatment with a mixture of concentrated sulfuric acid (H_2SO_4) and nitric acid (HNO_3) introduces oxygen-containing functional groups onto the CNT surface, thereby increasing its polarity and chemical reactivity (Scheme 1). During oxidation, the acid mixture attacks defect sites, tube ends, and, under sufficiently severe conditions, the sidewalls of CNTs. HNO_3 acts as a strong oxidizing agent, while concentrated H_2SO_4 contributes to the strongly acidic and dehydrating environment and can promote the formation of reactive oxidizing species. As a result, carbon atoms at energetically favorable sites are oxidized and converted into functional groups such as carboxyl, hydroxyl, and carbonyl groups. Carboxyl groups are particularly important because they can subsequently participate in covalent coupling reactions with polymers, amines, metals, or other functional molecules.[25]



Scheme 1. Schematic illustration of the functionalization of carbon nanotubes (CNTs)

The treatment of CNTs with urea after oxidative functionalization can be understood as a two-stage surface-engineering process. First, oxidation introduces reactive oxygen–containing groups onto the CNT surface. Second, urea interacts with these activated sites to produce urea–CNT composites with improved surface functionality, wettability, dispersion, and potentially biological activity.

3.1. *XRD analysis*

XRD was used to examine the crystallinity and layered structural properties of the starting materials (pristine CNTs and pure urea), the urea–CNT composite, and the CNT–urea–CNT composite (Figure 1).

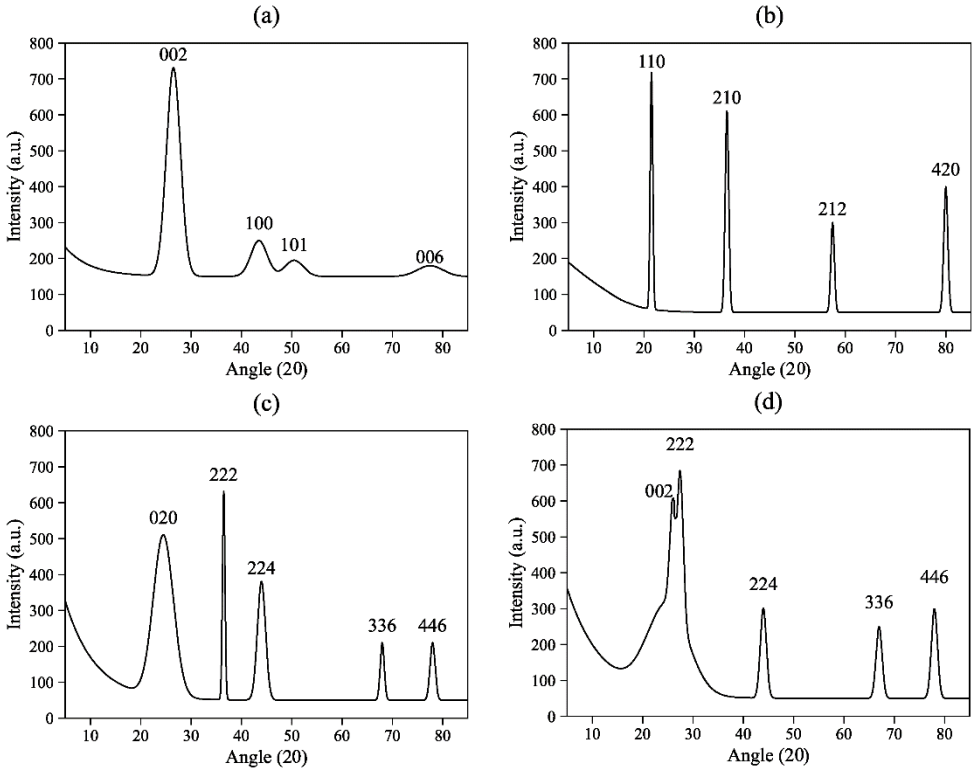


Fig. 1. X-ray diffraction (XRD) patterns of (a) pristine carbon nanotubes (CNTs), (b) pure urea, (c) the urea–CNT composite, and (d) the CNT–urea–CNT composite

Pristine CNTs present reflection peaks at approximately 2θ = 26°, 43°, 50°, and 77° (Figure 1a), which align with the (002), (100), (101), and (006) crystallographic planes, respectively.[24] The peak at 26° (2θ), indexed as the (002) reflection, is the most intense and sharp peak, indicating a high degree of graphitization. This corresponds to the interlayer spacing of graphite-like structures (3.4 Å), characteristic of the graphitic walls in CNTs. A sharp and intense peak here implies well-ordered multi-walled CNTs with good crystalline nature in the stacking direction. Additional weaker peaks – (100), (101), and (006) – support the presence of a partially crystalline, hexagonal graphitic structure typical of multi-walled CNTs. Overall, the pristine CNTs appear to be well-structured with some degree of crystallinity, common in high-quality synthesized CNTs.[26]

The XRD pattern of pure urea in Figure 1b shows major peaks at 2θ = 22°, 35°, 58°, and 78°. These peaks align with the crystal planes (110), (210), (212), and (420), respectively, which are consistent with the orthorhombic crystal system of urea. The observed peak at 2θ = 22°, indexed as (110), is the most intense peak, suggesting a preferred orientation or high crystallinity along the (110) plane.[27] The second peak at 35° (210) is a secondary high-intensity peak, indicating a prominent (210) reflection. The peak at 2θ = 58º, indexed as (212), supports the ordered structure of the urea crystal lattice. The peak at 2θ = 78º, indexed as (420), confirms the presence of fine periodicities in the crystal.

Figure 1c shows the XRD pattern of the urea–CNT composite. The peaks at 2θ = 22°, 35°, 43°, 65° and 79°—corresponding to the crystal planes (020), (222), (224), (336), and (446), respectively—reflect distinct crystal orientations, likely originating from well-crystallized urea. The intense reflection at approximately 35° (222) is the dominant peak in the pattern. Its enhanced relative intensity may be associated with preferential orientation of the urea crystallites.[28] The remaining reflections at approximately 43°, 65°, and 79°, indexed as (224), (336), and (446), respectively, further support the presence of an ordered crystalline urea phase. CNTs typically exhibit a broad diffraction feature near 2θ = 22°, commonly assigned to the (002) reflection of graphitic carbon. In the present composite pattern, this feature is weak or overlapped by the diffraction peaks associated with the urea phase. This may reflect the relatively low CNT content, the comparatively strong diffraction from crystalline urea, or the structural disorder associated with the CNT component.

The XRD pattern of the CNT–urea–CNT composite is shown in Figure 1d. A broad diffraction feature centered at approximately 2θ = 26°, indexed as

the (002) reflection, is characteristic of graphitic carbon and is consistent with the presence of CNTs. The breadth of this feature may be associated with structural disorder and/or the relatively small coherent crystallite size of the graphitic domains.[29] A sharp and intense reflection at approximately 2θ = 27°, indexed as (222), indicates the presence of a comparatively well-crystallized phase, which may be attributed to the diamide component.[30] That indicates a possible cubic or orthorhombic crystal structure of the diamide or a metal-organic framework derived from it.

3.2. *FTIR spectroscopy*

The FTIR spectra in the Figure 2 provide evidence for the presence of the characteristic functional groups of urea, oxidized CNTs, and the changes occurring after interaction between urea and CNTs. The spectrum of pure urea in Figure 2a shows the characteristic absorption bands associated with its amide functional groups. The broad band centered at approximately 3451 cm^{-1} is attributed mainly to N–H stretching vibrations of the $–NH_2$ groups. The band at approximately 1632 cm^{-1} corresponds to the C=O stretching vibration of the carbonyl group in urea.[31] In addition, the absorption around 1211 cm^{-1} is assigned to C–N stretching, which is characteristic of the urea structure. Thus, the bands at 3451, 1632, and 1211 cm^{-1} confirm the presence of the expected N–H, C=O, and C–N groups in urea.

Figure 2b shows the FTIR spectrum of CNTs, which includes bands associated with oxygen-containing surface groups and the carbon framework. The broad absorption at approximately 3435 cm^{-1} is attributed to O–H stretching, indicating the presence of hydroxyl groups, most likely generated during oxidative treatment of the CNTs. The bands at approximately 2925 and 2850 cm^{-1} are associated with aliphatic $C–H/CH_2$ stretching vibrations.[32] The absorption around 1635 cm^{-1} may be associated with C=O stretching from carbonyl/carboxyl surface functionalities and/or contributions from the graphitic carbon framework. The band near 1570 cm^{-1} is assigned to C=C stretching of the sp^2-hybridized carbon network, characteristic of the CNT structure. The band at approximately 1381 cm^{-1} is attributed to C–O-related vibrations.

The spectrum of the urea–CNT composite in Figure 2c shows contributions from both the CNT surface and urea. A broad band at approximately 3498 cm^{-1} is assigned to N–H stretching of $–NH_2$ groups, indicating the presence of urea-derived nitrogen-containing functionalities. The band at approximately 1750 cm^{-1} is assigned to C=O stretching, while the band around 1620 cm^{-1} is associated with N–H bending/stretching vibrations and may also contain contributions from the carbonyl/graphitic environment. The absorption at approximately 1218 cm^{-1}, assigned to C–N stretching, further supports the presence of urea-derived functionality on or associated with the surface.[31] Importantly, the appearance of N–H and C–N bands together with changes in the carbonyl region compared with pristine CNTs indicates that urea has interacted with the functionalized CNT surface. However, FTIR spectroscopy alone should be used to support the presence of these functional groups rather than as definitive proof of a specific covalent bonding mechanism.

The FTIR spectrum of the CNT–urea–CNT composite (Figure 2d) again shows several characteristic features resulting from CNT and urea. The broad band at approximately 3521 cm^{-1} is attributed to O–H stretching, indicating that hydroxyl groups remain present on the CNT surface. The bands at 2915 and 2855 cm^{-1} correspond mainly to $C–H/CH_2$ stretching vibrations. A band at around 2150 cm^{-1} is assigned to a cumulene/unsaturated carbon-related vibration. This band should be interpreted with caution because the region around 2100–2200 cm^{-1} can contain contributions from several less-common carbon functionalities and is not, by itself, sufficient to establish a particular structure. Most importantly, the absorption at approximately 1655 cm^{-1} is assigned to amide C=O stretching, while the band at approximately 1251 cm^{-1} is attributed to C–N stretching of an amide-type environment. The simultaneous observation of these bands suggests the formation or presence of amide-related functional groups in the CNT–urea–CNT composite.[33]

The shift and modification of the C=O, N–H, and C–N absorption bands after treatment of CNTs with urea indicate substantial interaction between urea and the functionalized CNT surface. In particular, the appearance of the bads at ~1655 cm^{-1} (C=O) and ~1251 cm^{-1} (C–N) in the CNT–urea–CNT composite is consistent with an amide-containing chemical environment.[34]

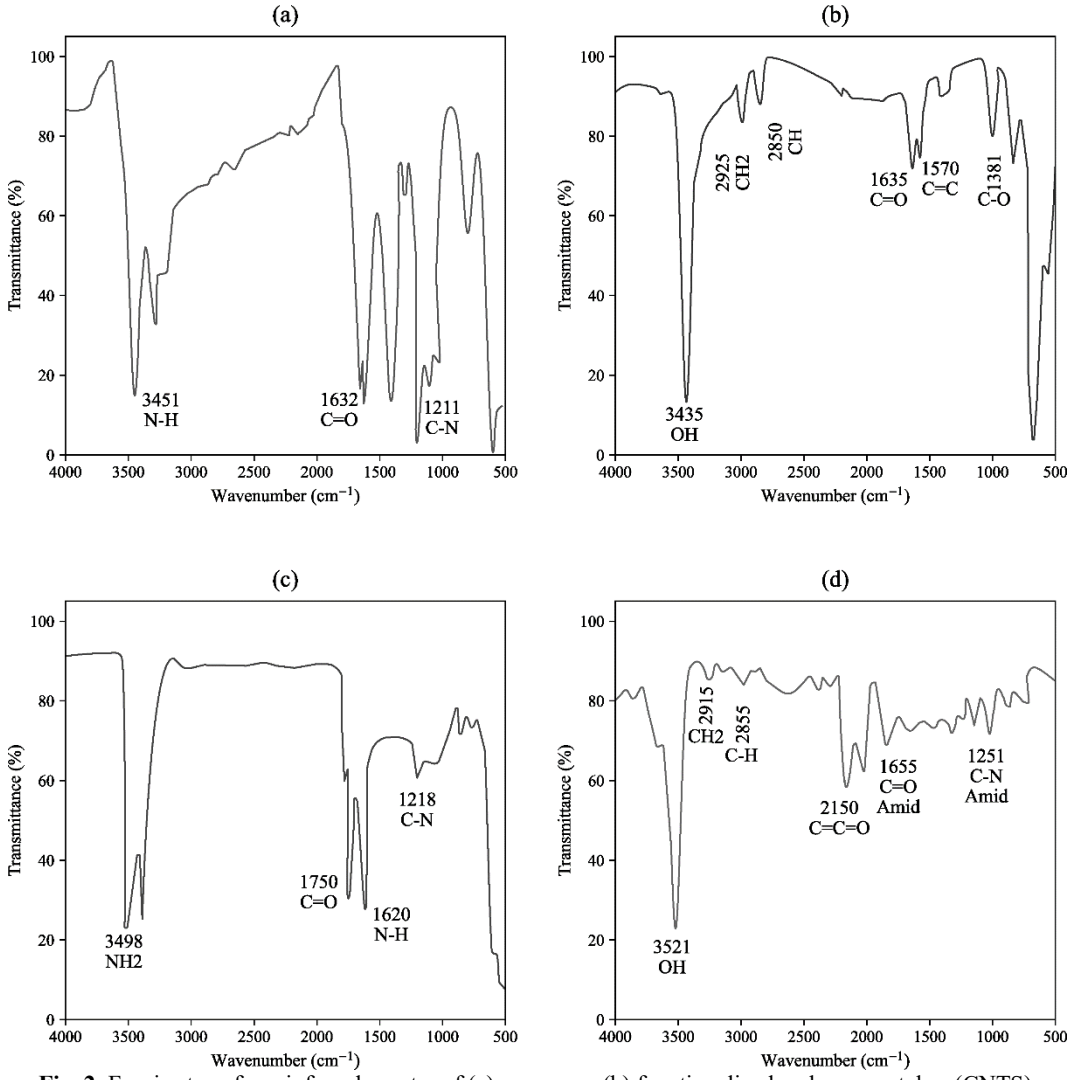


Fig. 2. Fourier-transform infrared spectra of (a) pure urea, (b) functionalized carbon nanotubes (CNTS), (c) the urea–CNT composite, and (d) the CNT–urea–CNT composite

3.3. *XPS analysis*

The high-resolution XPS spectra in Figure 3a reveal the characteristic C 1s and O 1s signals of pristine CNTs at approximately 284–285 and 532–534 eV, respectively. CNTs are mainly composed of carbon, with a relatively low oxygen content from oxygen-containing surface functionalities and limited surface oxidation. Following treatment with urea, a new peak appears at approximately 399–401 eV, corresponding to the N 1s region. The appearance of this nitrogen signal indicates the presence of nitrogen-containing species associated with the CNT surface and is consistent with the introduction or surface association of urea-derived species.[35]

The high-resolution C 1s spectra presented in Figure 3b are dominated by a peak centered near 284.5 eV, which is assigned to sp^2-hybridized C=C/C–C bonds characteristic of the graphitic CNT structure. Additional contributions at higher binding energies are associated with different oxygen- and nitrogen-containing groups on the surface, including C–C/C–N, C–O, C=O, and O–C=O groups. The presence of a contribution attributable to C–N environments, together with changes in the relative intensities of the carbon-containing components, is consistent with an altered chemical environment at the CNT surface following urea treatment. However, these changes alone cannot establish whether urea is covalently bound to the CNT framework or associated with the surface through noncovalent interactions. Therefore, the C 1s results are interpreted as supporting a modification of the surface chemical environment rather than providing definitive evidence of covalent functionalization.

The O 1s spectra shown in Figure 3c also reveal differences between pristine CNTs and the urea–CNT composite. For pristine CNTs, the broad O 1s feature can be primarily assigned to oxygen-containing surface groups, including C–O, C=O, and O–C=O. These groups may originate from the

preparation or mild oxidation of the CNT surface. After urea treatment, the O 1s envelope of the urea–CNT composite becomes more complex and can be separated into several components, reflecting different oxygen chemical environments. C=O species generally have lower binding energies, whereas C–O/O–C=O functional groups and adsorbed oxygen-containing species have higher binding energies.[36] The changes in the relative intensities of these components suggest that treatment with urea alters the chemical environment of the CNT surface.

Further evidence for the presence of urea-derived species is provided by the N 1s spectrum (Figure 3d). In contrast to pristine CNTs, the urea–CNT composite exhibits a distinct N 1s signal in the 399–401 eV region, indicating the presence of nitrogen-containing species on the CNT surface. Deconvolution of the N 1s envelope produces two components located approximately at 399.5–400.0 and 400.5–401.0 eV. These contributions may be associated with different nitrogen chemical environments arising from urea-derived species interacting with or associated with the CNT surface.

Collectively, the appearance of the N 1s signal, together with the changes observed in the C 1s and O 1s spectra, supports the presence of urea-derived nitrogen-containing species and an altered surface chemical environment after urea treatment. However, the XPS results do not by themselves establish the formation of specific covalent bonds between urea and the CNT framework. Therefore, the material is described as urea-treated or urea-associated CNTs, and the XPS findings are interpreted as evidence of surface modification rather than definitive proof of covalent urea functionalization.

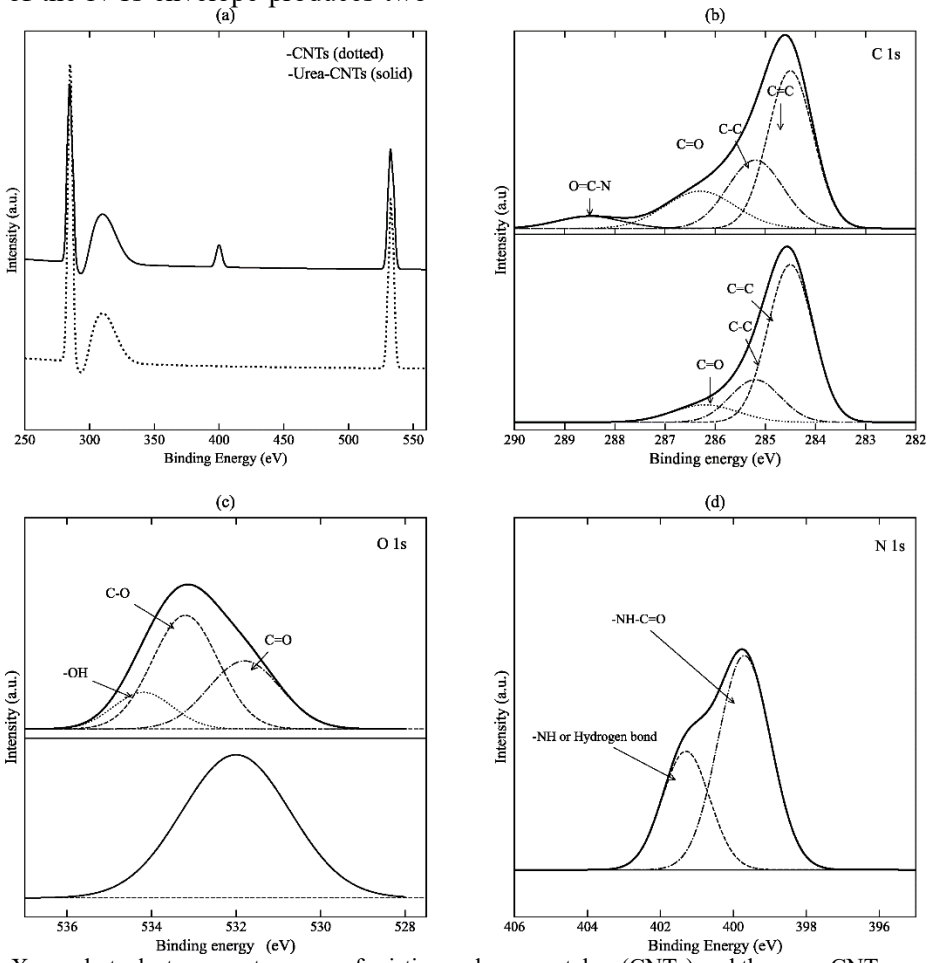


Fig. 3. X-ray photoelectron spectroscopy of pristine carbon nanotubes (CNTs) and the urea–CNT composite: (a) high resolution spectra, (b) C1s, (c) O1s, and (d) N1s

3.4. *TGA*

The TGA curves demonstrate a clear difference in the thermal stability of CNTs and urea-functionalized CNTs (Figure 4). CNTs exhibit high thermal stability, with negligible weight loss up to approximately 500 °C, followed by rapid mass loss between 550 and 680 °C corresponding predominantly to oxidative degradation of the CNT framework.[37] In comparison, the urea–CNT

composite shows earlier and more pronounced weight loss beginning at approximately 200–250 °C, with a major degradation step around 280–350 °C. This initial mass loss is attributed to the thermal decomposition of urea-derived surface functionalities and other weakly bound organic groups introduced during functionalization. The subsequent gradual decrease in mass at higher temperatures is associated with degradation of the CNT carbon framework. The earlier thermal decomposition of the urea–CNT composite compared with pristine CNTs confirms the presence of thermally labile urea-containing functional groups on the CNT surface. Overall, the TGA results support the successful functionalization of CNTs with urea and demonstrate that surface modification reduces their thermal stability.

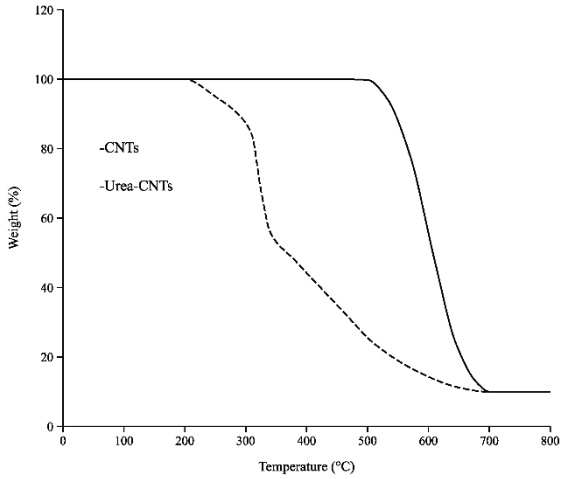


Fig. 4. Thermogravimetric analysis of pristine carbon nanotubes (CNTs) and the urea–CNT composite

3.5. *SEM*

Figure 5 presents SEM analysis, including a particle size distribution histogram, of the urea–CNT composite. SEM revealed a network of entangled CNTs with diameters ranging from 20 to 40 nm, forming a porous, web-like structure. Upon loading with urea, the surface of the CNTs appear coated with irregular, granular particles of crystallized urea, which are distributed unevenly along the CNT surface. Compared with pristine CNTs, which exhibit smooth and clean surfaces, the urea–CNT composite has a rougher texture, indicating successful deposition of urea. At higher magnification, the urea particles appear to partially agglomerate in localized regions, potentially due to hydrogen bonding and van der Waals interactions between urea and CNTs. There is no significant structural collapse or damage to the nanotube framework, suggesting that the composite preparation preserved the CNT integrity.[38] These observations confirm the physical adsorption and successful incorporation of urea onto the CNT matrix, potentially enhancing the surface reactivity and nitrogen content of the urea–CNT composite, which would make it useful for applications such as controlled-release fertilizers or chemical sensing.

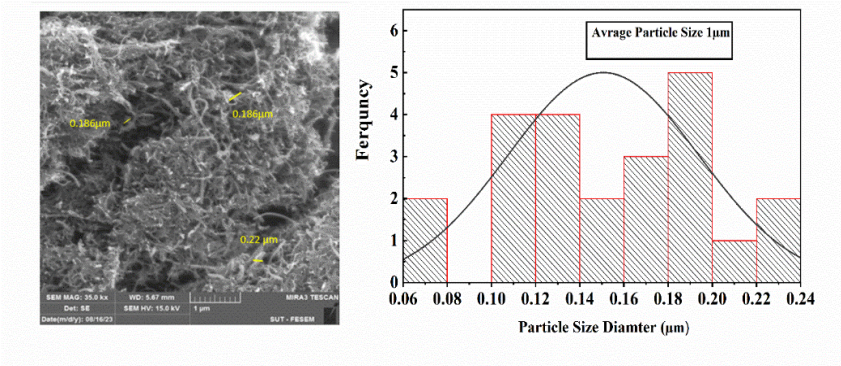


Fig. 5. Scanning electron microscopy analysis of the urea–carbon nanotube composite

Figure 6 presents SEM analysis, including a particle size distribution histogram, of the CNT–urea–CNT composite. These measurements suggest a relatively nanoscale dispersion of urea particles on the CNT framework. The particles appear to be irregularly shaped and clustered, which is typical in composites formed via physical or chemical deposition. The CNT network likely forms the darker, fibrous background, while urea particles appear as brighter, roughly spherical or elliptical formations. There is a relatively symmetric spread of particle sizes, with most particles 100–300 nm in diameter. The results confirm nanoscale integration and dispersion, which are critical for the material's potential performance in catalysis, adsorption, or electronic applications.

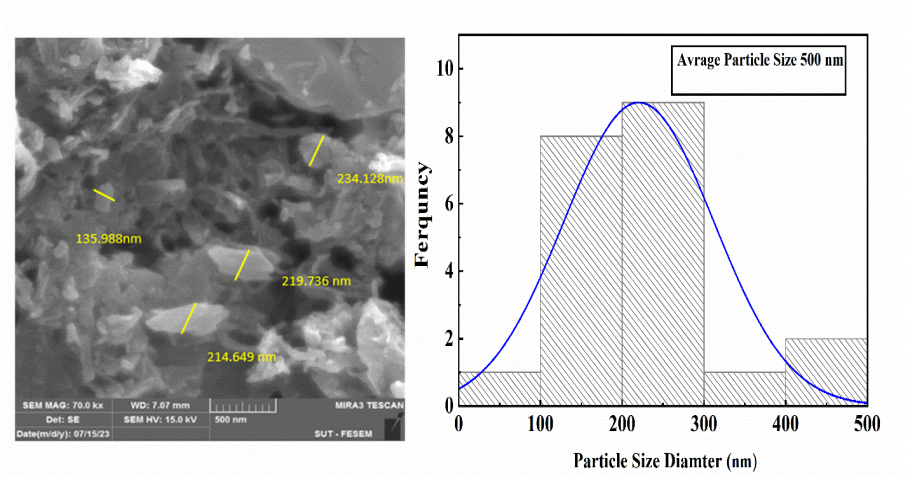


Fig. 6. Scanning electron microscopy analysis of the carbon nanotube–urea–carbon nanotube composite

3.6. *AFM*

Figure 7 presents an AFM image illustrating the surface topography of the urea–CNT composite, acquired using a scan size of 11.6 µm × 11.6 µm in Z-axis, scan forward, line fit mode. The image displays a distinct anisotropic pattern characterized by diagonally oriented, elongated bright regions. These bright regions correspond to areas with greater height, suggesting the presence of urea particles or aggregates deposited across the CNT surface. The dimmer, more continuous background with a smoother texture likely represents the underlying CNT network, which is known for its fibrous, cylindrical morphology. In AFM, CNTs generally appear as fine raised lines or bundles unless significantly coated.

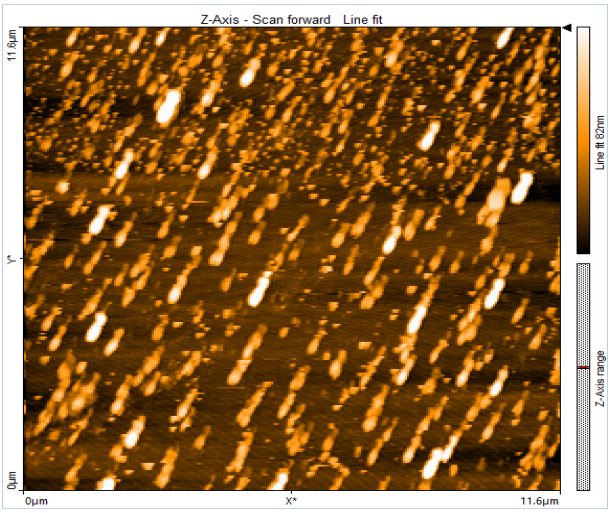


Fig. 7. Atomic force micrograph of the urea–carbon nanotube composite

The sharp and bright streaks indicate the formation of urea crystallites or clusters anchored onto the nanotubes.[39] The features exhibit variation in size and a nonuniform spatial distribution, consistent with heterogeneous nucleation and incomplete surface coverage. Overall, AFM verifies the successful incorporation of urea onto the CNT framework, showing nanoscale interaction and attachment, which may suggest potential interfacial bonding or adhesion between the two components.

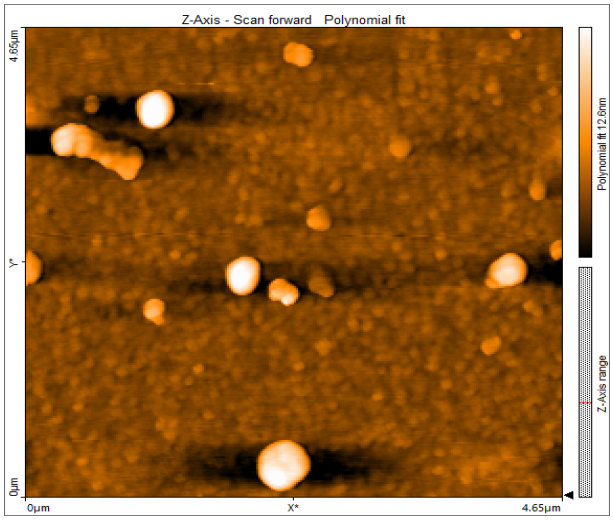


Fig. 8. Atomic force micrograph of the carbon nanotube–urea–carbon nanotube composite

The AFM image in Figure 8 shows the surface topography of the CNT–urea–CNT composite. Elongated, fibrous structures are distributed across the scanned surface, which are characteristic of CNT morphology. The CNTs appear more interconnected and sometimes bundled, suggesting cross-linking or aggregation, potentially due to diamide interaction. The nonuniform thickness or granular decorations on the CNTs suggests successful diamide functionalization, which can cause lead to great variation in height.

3.7. *Zeta potential*

The zeta-potential profiles presented in Figure 9 demonstrate a pronounced modification in the surface-charge characteristics of CNTs following urea treatment. Pristine CNTs (black curve) display a positive zeta potential under acidic conditions; it progressively decreases as pH increases. At approximately pH 2–4, the surface potential is approximately +60 mV. This gradual reduction in the zeta potential can be attributed to the increasing deprotonation of oxygen-containing surface functionalities as the pH rises. The zeta potential approaches and crosses the zero-potential region at approximately pH 7–8, indicating a point of zero charge/isoelectric point (PZC/IEP) of around pH 7.5 for pristine CNTs. At higher pH values, the CNT surface becomes progressively more negatively charged, reaching approximately −60 mV under strongly alkaline conditions.[40] This behavior is consistent with the presence of oxygen-containing surface groups, including –COOH, –OH, and C=O, which undergo pH-dependent protonation and deprotonation and can generate negatively charged surface sites, particularly deprotonated carboxylate groups.

The urea–CNT composite (red curve) exhibits a substantially different surface-charge profile. Under acidic conditions, the zeta potential is approximately +70 mV. It then decreases more rapidly as pH increases compared with pristine CNTs and crosses the zero-potential point at approximately pH 4, corresponding to an PZC/IEP around pH 4. Above this value, the urea–CNT composite becomes increasingly negatively charged, reaching approximately −90 mV at pH 12. The shift in the IEP from approximately pH 7–8 for pristine CNTs to around pH 4 after urea treatment indicates a substantial alteration of the surface-charge environment.[41] This change is consistent with the introduction or association of nitrogen-containing functionalities and changes in the hydrogen-bonding and protonation–deprotonation behavior at the CNT surface. Importantly, the zeta potential results demonstrate a change in the interfacial charge properties after urea treatment but do not, by themselves, establish the formation of covalent bonds between urea and CNTs.

The change in surface charge is also relevant to the observed antibacterial behavior because bacterial cell envelopes generally have an overall negative surface charge under physiological and near-neutral conditions. This negative charge originates from components such as phospholipids, teichoic acids in gram-positive bacteria, and lipopolysaccharides and phospholipids in gram-negative bacteria. Consequently, electrostatic interactions can influence the initial approach, adsorption, and association of charged nanomaterials with bacterial surfaces. The zeta potential results indicate that both CNT materials undergo substantial changes in surface charge with pH, while the urea–CNT composite becomes considerably more negatively charged than pristine CNTs at higher pH values. Although this increased negative charge would not be expected to promote simple electrostatic attraction toward the negatively charged bacterial envelope, it may modify the hydration layer, colloidal stability, interfacial interactions, and the availability of surface functional groups involved in hydrogen bonding and other non-electrostatic interactions. Therefore, surface charge should be considered as one component of a more complex CNT–bacteria interaction mechanism rather than as the sole determinant of antibacterial activity.

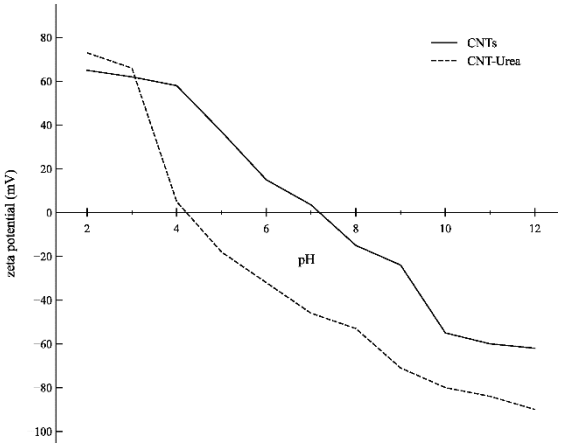


Fig. 9. Zeta potential of pristine carbon nanotubes (CNTs) and the urea–CNT composite

The inhibition zone results provide further evidence that the surface modification affects the interaction of the CNT-based materials with bacterial cells. The urea–CNT and CNT–urea–CNT composites inhibited *S. aureus* and *E. coli* in a concentration-dependent manner. At 0.1 mg mL^{-1}, the urea–CNT and CNT–urea–CNT composites produced inhibition zones of 25 ± 1.62 and 30 ± 2.08 mm, respectively, against *S. aureus*, and inhibition zones of 23 ± 2.06 and 33 ± 3.01 mm, respectively, against *E. coli*. The larger inhibition zones generally observed for the CNT–urea–CNT composite suggest that differences in surface characteristics, dispersion behavior, accessible functional groups, and/or interactions with bacterial cells may influence antibacterial performance. In particular, the modified surface chemistry and altered charge characteristics revealed by the zeta

potential measurements may facilitate closer interfacial association between the nanocomposite and bacterial cells, potentially promoting membrane perturbation or other surface-mediated antibacterial effects.

However, the relationship between zeta potential and the diameter of the inhibition zone should be interpreted with caution. Disk diffusion is influenced not only by antibacterial activity but also by the dispersion and mobility of CNT-based materials through the Mueller–Hinton agar matrix. Because CNTs are relatively large, anisotropic nanostructures and may form aggregates, their migration through the agar does not necessarily correspond directly to their concentration or intrinsic antibacterial potency. Therefore, the larger inhibition zones observed for the urea–CNT and CNT–urea–CNT composites cannot be attributed exclusively to their more negative zeta potentials. Instead, the results suggest that the altered surface-charge properties, together with the modified surface chemistry, dispersion characteristics, and direct nanomaterial–bacteria interactions, collectively contribute to the observed antibacterial response. Overall, the zeta-potential measurements provide complementary evidence that urea treatment substantially changes the interfacial properties of the CNT surface. When considered together with the concentration-dependent inhibition zones, these findings support the interpretation that modification of the CNT surface influences its interaction with bacterial cells.

3.8. *Antibacterial activity*

To assess antibacterial activity, the urea–CNT and CNT–urea–CNT composites and pristine CNTs were individually dispersed in distilled water. Suspensions of *S. aureus* and *E. coli* were prepared in sterile saline solution for testing (Figure 10). The dispersions were ultrasonicated for 30–60 minutes to ensure uniform distribution. Three concentrations were tested: 0.01, 0.05, and 0.1 mg mL^{-1}.

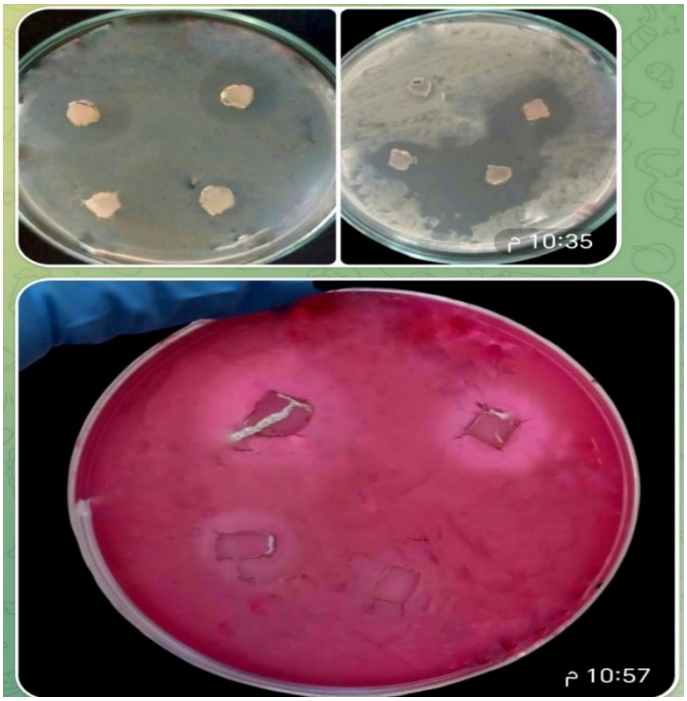


Fig. 10. Typical examples of plates used to assess the antibacterial activity of the urea–CNT and CNT–urea–CNT composites against *Staphylococcus aureus* and *Escherichia coli*

The urea–CNT and CNT–urea–CNT composites presented concentration-dependent antibacterial activity against *S. aureus* (Table 1). For the urea–CNT compositive, the inhibition zone decreased progressively as the concentration decreased: 25 ± 1.62 mm at 0.1 mg mL^{-1}, 20 ± 1.50 mm at 0.05 mg mL^{-1}, and 12 ± 1.00 mm at 0.01 mg mL^{-1}. Similarly, the CNT–urea–CNT composite exhibited its largest inhibition zone at the highest concentration tested: 30 ± 2.08 mm at 0.1 mg mL^{-1}, 22 ± 2.00 mm at 0.05 mg mL^{-1}, and just 8 ± 2.00 mm at 0.01 mg mL^{-1}. Thus, compared with the urea–CNT composite, the antibacterial activity of the CNT–urea–CNT composite was greater at 0.1 and 0.05 mg mL^{-1} but decreased substantially at the lowest concentration. The differences between the composites may be associated with variations in the surface architecture, dispersion characteristics, and interactions of the composites with bacterial cells.

Table 1. The antibacterial activity of the urea–carbon nanotube (CNT) and CNT–urea–CNT composites against *Staphylococcus aureus*

Compound	0.1 mg/ml	0.05 mg/ml	0.01mg/ml
S1	25 ± 1.62	20 ± 1.5	12 ± 1
S2	30 ± 2.08	22 ± 2	8 ± 2

The urea–CNT and CNT–urea–CNT composites also exhibited antibacterial activity against *E. coli*, with the CNT–urea–CNT composite demonstrating greater activity than the urea–CNT composite at all tested concentrations (Table 2). For the urea–CNT composite, the inhibition zone was 23 ± 206 mm at 0.1 mg mL^{-1}, 22 ± 1 mm at 0.05 mg mL^{-1}, and 9 ± 2.00 mm at 0.01 mg mL^{-1}. For the CNT–urea–CNT composite, the inhibition zone was 33 ± 3.01 mm at 0.1 mg mL^{-1}, 28 ± 2 m at 0.05 mg mL^{-1}, and 12 ± 1.00 mm at 0.01 mg mL^{-1}. This concentration-dependent pattern indicates that increasing the concentration of the functionalized CNT composites results in greater inhibition of *E. coli*. The relatively small difference in the inhibition zone for the urea–CNT composite between 0.1 and 0.05 mg mL^{-1} may suggest that its antibacterial effect approaches a plateau within this concentration range. The greater antibacterial activity observed for the CNT–urea–CNT composite may be associated with differences in its surface functionalization and physicochemical interactions with the bacterial cell envelope.[42] These findings suggest that the incorporation of urea/amide functionalities into CNTs may enhance their antibacterial performance, particularly at higher concentrations.

Table 2. The antibacterial activity of the urea–carbon nanotube (CNT) and CNT–urea–CNT composites against *Escherichia coli*

Compound	0.1 mg/ml	0.05 mg/ml	0.01 mg/ml
S1	23 ± 2.06	22 ±1	9 ± 2
S2	33 ± 3.01	28 ± 2	12 ± 1

4. CONCLUSION

In conclusion, urea treatment substantially modified the CNT surface, as supported by FTIR, XRD, XPS, TGA, SEM, AFM, and measurement of the zeta potential. The appearance of nitrogen- and amide-related spectral features, together with the changes observed in the C 1s, O 1s, and N 1s XPS regions, supports the incorporation of urea-derived functionalities onto the CNT surface. A limitation of the present study is that the available characterization results are not sufficient to conclusively establish covalent bonding between urea and CNTs; therefore, the observed interactions are interpreted as urea-associated surface functionalization, potentially involving hydrogen bonding and other noncovalent interactions. The shift in the IEP from approximately pH 7–8 for pristine CNTs to around pH 4 after urea treatment further confirms a pronounced change in surface-charge behavior and surface chemistry. Although urea treatment reduced the thermal stability of the composites, they exhibited notable antibacterial activity against both *S. aureus* and *E. coli*, with activity generally increasing with concentration. In particular, the CNT–urea–CNT composite demonstrated the strongest antibacterial performance against *E. coli*, producing an inhibition zone of 33 ± 3.01 mm at 0.1 mg mL^{-1}. Overall, the findings indicate that urea treatment provides an effective approach for modifying CNT surface properties and enhancing their antibacterial performance, while the observed differences between the urea–CNT composite and the CNT–urea–CNT composite highlight the importance of surface structure, dispersion, and bacterial–nanotube interactions in determining antimicrobial activity.

Acknowledgments: The authors would like to acknowledge Sulaimani University, College of Science, Chemistry department and Al-Iraqia University College of Education, for materials characterization, and laboratory Management, for research facilities and data analysis.

Funding The authors declare that no funds, grants, or other support were received during the preparation of this manuscript.

Data availability: The authors confirm that the data supporting the outcomes of this research are accessible within the article.

REFERENCES

(1) Iijima, S. Helical Microtubules of Graphitic Carbon. *Nature* **1991**, *354*, 56–58.

(2) Tasis, D.; Tagmatarchis, N.; Bianco, A.; Prato, M. Chemistry of Carbon Nanotubes. *Chem. Rev.* **2006**, *106* (3), 1105–1136.

(3) Lin, Y.; Taylor, S.; Li, H.; Fernando, K. A. S.; Qu, L.; Wang, W.; Gu, L.; Zhou, B.; Sun, Y.-P. Advances toward Bio Applications of Carbon Nanotubes. *J. Mater. Chem.* **2004**, *14*, 527–541.

(4) Tan, J. M.; Arulselvan, P.; Fakurazi, S; Ithnin, H.; Hussein, M. Z. A Review on Characterizations and Biocompatibility of Functionalized Carbon Nanotubes in Drug Delivery Design, *Journal of Nanomaterials*, **2014**, 917024, 20 pages. https://doi.org/10.1155/2014/917024.

(5) Dubey, R.; Dutta, D.; Sarkar, A.; Chattopadhyay, P. Functionalized Carbon Nanotubes: Synthesis, Properties and Applications in Water Purification, Drug Delivery,

and Material and Biomedical Sciences. *Nanoscale Adv.* **2021**, *3*, 5722–5744.

(6) Chang, R. Y. K.; Nang, S. C.; Chan, H.-K.; Li, J. Novel Antimicrobial Agents for Combating Antibiotic-Resistant Bacteria. *Adv. Drug Delivery Rev.* **2022**, *187*, 114378.

(7) Roldo, M.; Fatouros, D. G. Biomedical Applications of Carbon Nanotubes. *Annu. Rep. Prog. Chem., Sect. C: Phys. Chem.* **2013**, *109*, 10–35.

(8) Khalaf, Q. Z.; Mohsen, M. K.; Al-Salihi, K. J. J.; Omer, R. A.; Azeez, Y. H. Synthesis and Density Functional Theory Study on the Functionalization of Carbon Nanotube Conjugates with Amino Compounds and Their Application in Dyeing Processes. *ChemistrySelect* **2024**, *9* (25), e202403525.

(9) Vardharajula, S.; Ali, S. Z.; Tiwari, P. M.; Eroğlu, E.; Vig, K.; Dennis, V. A.; Singh, S. R. Functionalized Carbon Nanotubes: Biomedical Applications. *Int. J. Nanomed.* **2012**, *7*, 5361–5374. https://doi.org/10.2147/IJN.S35832

(10) Bianco, A.; Kostarelos, K.; Prato, M. Applications of Carbon Nanotubes in Drug Delivery. *Curr. Opin. Chem. Biol.* **2005**, *9* (6), 674–679.

(11) Kang, S.; Mauter, M. S.; Elimelech, M. Physicochemical Determinants of Multiwalled Carbon Nanotube Bacterial Cytotoxicity. *Environ. Sci. Technol.* **2008**, *42* (19), 7528–7534. https://doi.org/10.1021/es8010173

(12) Gatoo, M. A.; Naseem, S.; Arfat, Mir Y.; Mahmood D.; Ayaz, Qasim, K.; Zubair, S. Physicochemical Properties of Nanomaterials: Implication in Associated Toxic Manifestations, *BioMed Res. Int.* **2014**, 498420, 8 pages. https://doi.org/10.1155/2014/498420.

(13) Olivi, M.; Zanni, E.; De Bellis, G.; Talora, C.; Sarto, M. S.; Palleschi, C.; Flahaut, E.; Monthioux, M.; Rapino, S.; Uccelletti, D.; Fiorito, S. Inhibition of Microbial Growth by Carbon Nanotube Networks. *Nanoscale* **2013**, *5* (19), 9023–9029.

(14) Kang, S.; Mauter, M. S.; Elimelech, M. Microbial Cytotoxicity of Carbon-Based Nanomaterials: Implications for River Water and Wastewater Effluent. *Environ. Sci. Technol.* **2009**, *43*, 2648–2653.

(15) Abo-Neima, S. E.; Motaweh, H. A.; Elsehly, E. M. Antimicrobial Activity of Functionalized Carbon Nanotubes against Pathogenic Microorganisms. *IET Nanobiotechnol.* **2020**, *14* (6), 457–464.

(16) Ji, H.; Sun, H.; Qu, X. Antibacterial Applications of Graphene-Based Nanomaterials: Recent Achievements and Challenges. *Adv. Drug Delivery Rev.* **2016**, *105*, 176–189.

(17) Prasad, K.; Lekshmi, G. S.; Ostrikov, K.; Lussini, V.; Blinco, J.; Mohandas, M.; Vasilev, K.; Bottle, S.; Bazaka, K.; Ostrikov, K. Synergic Bactericidal Effects of Reduced Graphene Oxide and Silver Nanoparticles against Gram-Positive and Gram-Negative Bacteria. *Sci. Rep.* **2017**, *7*, 1591.

(18) Moskvitina, E.; Kuznetsov, V.; Moseenkov, S.; Serkova, A.; Zavorin, A. Antibacterial Effect of Carbon Nanomaterials: Nanotubes, Carbon Nanofibers, Nanodiamonds, and Onion-like Carbon. *Materials* **2023**, *16* (3), 957. https://doi.org/10.3390/ma16030957

(19) Li, H.; He, X.; Liu, Y.; Huang, H.; Lian, S.; Lee, S.-T. One-Step Ultrasonic Synthesis of Water-Soluble Carbon Nanoparticles with Excellent Photoluminescent Properties. *Carbon* **2011**, *49*, 605–609.

(20) Saeed, K.; Park, S.-Y. Preparation and Characterization of Multiwalled Carbon Nanotubes/Polyacrylonitrile Nanofibers. *J. Polym. Res.* **2010**, *17*, 535–540. https://doi.org/10.1007/s10965-009-9341-4

(21) Bauer, A. W.; Kirby, W. M.; Sherris, J. C.; Turck, M. Antibiotic Susceptibility Testing by a Standardized Single Disk Method. *Am. J. Clin. Pathol.* **1966**, *45*, 493–496.

(22) Khan, Z. A.; Siddiqui, M. F.; Park, S. Current and Emerging Methods of Antibiotic Susceptibility Testing. *Diagnostics* **2019**, *9*, 49.

(23) González-Sánchez, M.; Valera, J. S.; Veiga-Herrero, J.; Chamorro, P. B.; Aparicio, F.; González-Rodríguez, D. Self-Assembled Nanotubes from the Supramolecular Polymerization of Discrete Cyclic Entities. *Chem. Soc. Rev.* **2025**, *54*, 5657–5697.

(24) Díez-Pascual, A. M. Chemical Functionalization of Carbon Nanotubes with Polymers: A Brief Overview. *Macromol.* **2021**, *1*, 64–83. https://doi.org/10.3390/macromol1020006

(25) Gerber, I.; Oubenali, M.; Bacsa, R.; Durand, J.; Gonçalves, A.; Pereira, M. F. R.; Jolibois, F.; Perrin, L.; Poteau, R.; Serp, P. Theoretical and Experimental Studies on the Carbon-Nanotube Surface Oxidation by Nitric Acid: Interplay between Functionalization and Vacancy Enlargement. *Chem. Eur. J.* **2011**, *17*, 11467–11477. https://doi.org/10.1002/chem.201101438

(26) Das, R.; Abd Hamid, S. B.; Ali, M. E.; Ramakrishna, S.; Yongzhi, W. Carbon Nanotubes Characterization by X-ray Powder Diffraction – A Review. *Curr. Nanosci.* **2015**, 11 (1).

(27) Oddershede, J.; Nielsen, K.; Stahl, K. Using X-ray Powder Diffraction and Principal Component Analysis to Determine Structural Properties for Bulk Samples of Multiwall Carbon Nanotubes. *Z. Kristallogr.* **2007**, *222*, 186–192.

(28) Hammond, R.; Pencheva, K.; Roberts, K. J.; Mougin, P.; Wilkinson, D. An Examination of the Thermal Expansion of Urea Using High-Resolution Variable-Temperature X-ray Powder Diffraction. *J. Appl. Crystallogr.* **2005**, *38*, 1038–1039.

(29) Cavness, B.; Heimbecker, J.; Velasquez III, J., V.; Williams, S. X-ray Fluorescence as a Method of Monitoring Metal Catalyst Content during the Purification of Carbon Nanotubes. *Radiat. Phys. Chem.* **2012**, *81* (2), 131–134.

(30) García-Gutiérrez, M. C.; Nogales, A.; Hernández, J. J.; Rueda, D. R.; Ezquerra, T. A. X-ray Scattering Applied to the Analysis of Carbon Nanotubes, Polymers and Nanocomposites. *Opt. Pura Apl.* **2007**, *40* (2), 195–205.

(31) Maiti, K. S. Ultrafast N–H Vibrational Dynamics of Hydrogen-Bonded Cyclic Amide Reveal by 2DIR Spectroscopy. *Chem. Phys.* **2018**, *515*, 509–512.

(32) Naeimi, H.; Mohajeri, A.; Moradi, L.; Morad Rashidi, A. Solubilization of Multi Walled Carbon Nanotubes under a Facile and Mild Condition. *J. Nanosci. Nanotechnol.* **2011**, *11*, 1–4.

(33) Yatim, M.; Shaaban, N.; Dimin, A.; Yusof, M. F.; Abd Razak, F.; Jeefferie, A. R. Application of Response Surface Methodology for Optimization of Urea Grafted Multiwalled Carbon Nanotubes in Enhancing Nitrogen Use Efficiency and Nitrogen Uptake by Paddy Plants. *J. Nanotechnol.* **2016**, *2016*, 1250739. https://doi.org/10.1155/2016/1250739

(34) Yatim, N. M.; Shaaban, A.; Dimin, M. F.; Yusof, F.; Razak, J. A. Effect of Functionalised and Non-Functionalised Carbon Nanotubes-Urea Fertilizer on the Growth of Paddy. *Trop. Life Sci. Res.* **2018**, *29* (1), 17–35. https://doi.org/10.21315/tlsr2018.29.1.2

(35) Wang, Y.; Hu, Q.; Ye, M.; Huang, X.; Chen, Q.; Hu, C. Synergistic Flame Retardancy of Epoxy Resin with Aminated Multi-Walled Carbon Nanotubes and Ammonium Polyphosphate. *Polymers* **2026**, *18* (10), 1158. https://doi.org/10.3390/polym18101158

(36) Xu, S.; Lu, R.; Sun, K.; Tang, J.; Cen, Y.; Luo, L.; Wang, Z.; Tian, S.; Sun, X. Synergistic Effects in N,O-Comodified Carbon Nanotubes Boost Highly Selective Electrochemical Oxygen Reduction to H_2O_2. *Adv. Sci.* **2022**, *9*, 2201421. https://doi.org/10.1002/advs.202201421

(37) Trakakis, G.; Tomara, G.; Datsyuk, V.; Sygellou, L.; Bakolas, A.; Tasis, D.; Parthenios, J.; Krontiras, C.; Georga, S.; Galiotis, C.; Papagelis, K. Mechanical, Electrical, and Thermal Properties of Carbon Nanotube Buckypapers/Epoxy Nanocomposites Produced by Oxidized and Epoxidized Nanotubes. *Materials* **2020**, *13* (19), 4308. https://doi.org/10.3390/ma13194308

(38) Krasley, A. T.; Li, E.; Galeana, J. M.; Bulumulla, C.; Beyene, A. G.; Demirer, G. S. Carbon Nanomaterial Fluorescent Probes and Their Biological Applications. *Chem. Rev.* **2024**, *124*, 3085–3185.

(39) Slattery, A. D.; Shearer, C. J.; Shapter, J. G.; Blanch, A. J.; Quinton, J. S.; Gibson, C. T. Improved Application of Carbon Nanotube Atomic Force Microscopy Probes Using Peak Force Tapping Mode. *Nanomaterials* **2018**, *8*, 807. https://doi.org/10.3390/nano8100807

(40) Skwarek, E.; Bolbukh, Y.; Tertykh, V.; Janusz, W. Electrokinetic Properties of the Pristine and Oxidized MWCNT Depending on the Electrolyte Type and Concentration. *Nanoscale Res. Lett.* **2016**, *11* (1), 166. https://doi.org/10.1186/s11671-016-1367-z

(41) Chen, L.; Xie, H.; Li, Y.; Yu, W. Surface Chemical Modification of Multiwalled Carbon Nanotubes by a Wet-Mechanochemical Reaction. *J. Nanomater.* **2008**, 783981. https://doi.org/10.1155/2008/783981

(42) Zakharova, O. V.; Gusev, A. A.; Baranchikov, P. A.; Chebotaryova, S. P.; Razlivalova, S. S.; Koiava, E. Y.; Kataranova, A. A.; Grigoriev, G. V.; Strekalova, N. S.; Krutovsky, K. V. The Composition of the Dispersion Medium Determines the Antibacterial Properties of Copper(II) Oxide Nanoparticles against Escherichia coli Bacteria. *Nanomaterials* **2025**, *15*, 469. https://doi.org/10.3390/nano15060469